



# Photospheric vortex flows close to the polarity inversion line of a fully emerged active region

Jean C. Santos<sup>1</sup> and Cristiano M. Wrasse<sup>2</sup>

<sup>1</sup>Universidade Tecnológica Federal do Paraná, Curitiba-PR, Brazil.

<sup>2</sup>Instituto Nacional de Pesquisas Espaciais, São José dos Campos-SP, Brazil.

**Correspondence:** Jean C. Santos ([jeansantos@utfpr.edu.br](mailto:jeansantos@utfpr.edu.br))

**Abstract.** We report on the occurrence of vortices in flow fields obtained from the evolution of the line-of-sight component of the photospheric magnetic field in a region around the polarity inversion line of a fully emerged active region. Based on a local linear approximation for the flow field, we identify the presence of critical points and classify them according to the eigenvalues of the Jacobian matrix of the linear transformation. Vortices are associated to the presence of a particular kind of critical point, known as Attracting Focus. Using this method we identified twelve vortices in the analyzed period and detected the occurrence of other types of critical points, which indicate the complexity of the flow field around the PIL. The detected vortices show a clockwise preferred sense of rotation with approximately 67% of the cases. A geometrical analysis of the velocity structures produced an average value of  $\bar{D} = 1.63 \pm 0.05$  for the fractal dimension, which is very close to the one obtained for isotropic homogeneous turbulence ( $D = 5/3$ ). This suggests that the flow around the polarity inversion line is turbulent in nature.

10 *Copyright statement.* TEXT

## 1 Introduction

Horizontal flow fields in the solar photosphere have an important role in the concentration and dispersal of surface magnetic flux. Just to give some examples, surface flows are responsible for magnetic flux concentration at the border of the convection cells (magnetic network); they disperse the magnetic flux of active regions (turbulent diffusion); and they transport the magnetic flux to the poles (meridional flow). Horizontal flows may also contribute to magnetic energy and helicity injection into the upper atmosphere by twisting and interweaving the footpoints of flux-tubes, generating field aligned currents and magneto-hydrodynamic waves, and also may be responsible for the occurrence of magnetic reconnection by bringing together opposite magnetic polarity regions. Therefore, the investigation of photospheric horizontal motion patterns responsible for the evolution of magnetic features in the solar photosphere may give some clues to understand how the combination of these two quantities, magnetic field and flow field, influence the solar activity.

In this sense, vortex/rotational motion patterns are particularly important for solar activity. In the quiet Sun convective flows concentrate magnetic fields in the downdraft region of the convective cells. The conservation of angular momentum forces the



plasma to rotate around the center of the downdraft, generating small scale vortices. These vortices have been extensively detected in observations of the photosphere (Brandt et al., 1988; Simon and Weiss, 1997; Attie et al., 2009; Bonet et al., 2010; Balmaceda et al., 2010; Vargas Domínguez et al., 2011) and also have been observed in the quiet Sun chromosphere as a signature of plasma moving along curly magnetic field lines in coronal holes (Wedemeyer-Böhm and Rouppe van der Voort, 2009). Simulations indicate that the vortices occurring in strongly magnetized regions are closely connected with dissipation processes providing localized heating in the lower parts of the solar atmosphere (Moll et al., 2012) and observations show that the vortices are indeed associated to the occurrence of bright points (Bonet et al., 2008).

On larger scales, rotational motions were observed in sunspots and they are usually associated with energy and helicity build-up and later release by flare and/or coronal mass ejection (Brown et al., 2003; Hiremath and Suryanarayana, 2003; Hiremath et al., 2005; Yan and Qu, 2007; Yan et al., 2008; Min and Chae, 2009; Yan et al., 2009; Kazachenko et al., 2010; Zhu et al., 2012; Yan et al., 2012; Jiang et al., 2012; Vemareddy et al., 2012; Hardersen et al., 2013; Wang et al., 2014; Ruan et al., 2014; Gopasyuk, 2015; Li and Liu, 2015; Suryanarayana et al., 2015; Wang et al., 2016; Vemareddy et al., 2016). The rotation of sunspots is usually very slow, this means that the evolution of the magnetic field in the corona associated to it would be slow as well. However, strong flares (M- or X-class) are usually associated to rapid (abnormal) sunspot rotation. At the moment there is not a defined mechanism to explain sunspot rotation. It is suggested that it could be a result of the interaction of the flux tube with photospheric flows, during or after its emergence, or the effect of the emergence of a twisted flux tube. Changes of rotational pattern of sunspot after the flare occurrence were also observed (Liu et al., 2016; Bi et al., 2016) and they are associated to Lorentz forces.

In this work, we investigate the properties of the flow field obtained from the evolution of photospheric magnetic features around the polarity inversion line (PIL) of a fully emerged active region (AR9289). We targeted the PIL since it is the place where opposite polarity magnetic fields interact and where sharp changes are usually associated to the onset of flares (Severnyi, 1958; Wang et al., 1994; Kosovichev and Zharkova, 2001; Sudol and Harvey, 2005; Sharykin et al., 2017). We first investigate the geometric structure of the flow, by calculating its the fractal dimension, and use it to check if the flow around PIL presents turbulent nature. Finally, we focus in the detection and classification of critical points. Critical points are points where the velocity vanishes and their importance resides in the fact that the flow may be directed to and rotate around these points forcing opposite polarities to meet and annihilate there, contributing to the energetics of the solar atmosphere. The critical points are used to identify the presence of vortex flows in the region around the polarity inversion line.

## 2 Data and methodology

We selected as our target the active region NOAA 9289, located at the southern solar hemisphere. Figure 1 shows the full disk line-of-sight (LOS) component of photospheric magnetic field (top panel) and a close view of AR9289 (bottom panel), as measured by the Michelson Doppler Imager (MDI) (Scherrer et al., 1995) on January 2<sup>nd</sup> 2001 at 04:51:01 UT. The LOS magnetic field ( $B_{LOS}$ ) is saturated at  $\pm 100$  G for a better visualization of the magnetic features. The active region consisted of a large bipolar magnetic field with a leading negative polarity and a following positive polarity region. From December 31<sup>st</sup>



2000 to January 3<sup>rd</sup> 2001 the region was fully emerged and its leading sunspot was seen to rotate about 50° clockwise with an average speed of 0.56° h<sup>-1</sup> (Zhu et al., 2012). As shown in Figure 1, there was a smaller bipolar region located close to AR9289. We focus in a region of approximately 54x78 arcsec<sup>2</sup> around the PIL and follow the evolution of  $B_{LOS}$  for a period of 3.6 days

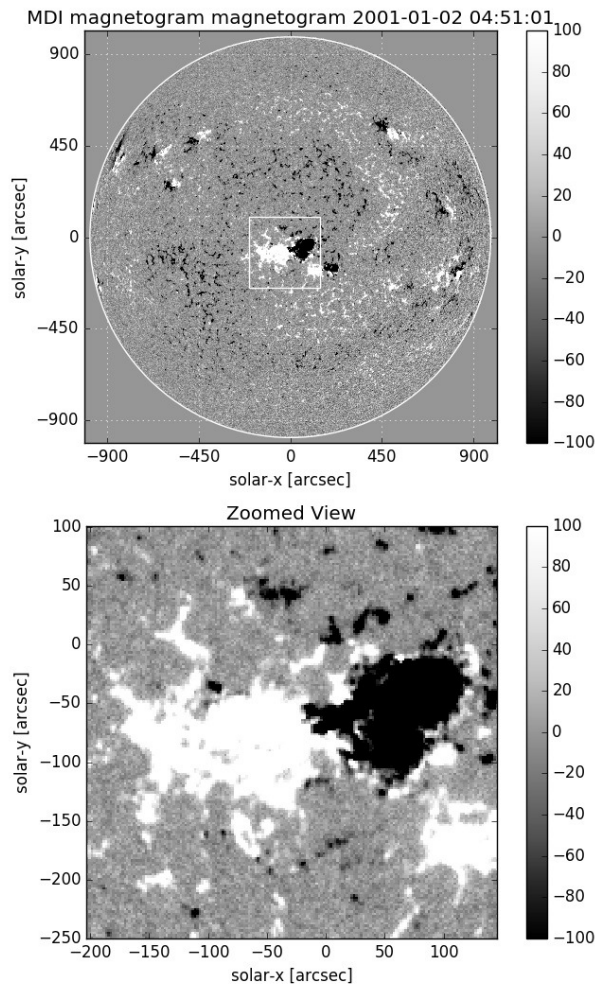


**Figure 1.** Full disk LOS magnetic field (top panel) and close view of AR9289 (bottom panel) as measured by the MDI/SoHO instrument on January 2<sup>nd</sup> 2001 at 04:51:01 UT.

starting on December 31<sup>st</sup> 2000 at 01:34:43 UT. Figure 2 display the  $B_{LOS}$  measurements with a cadence of 192 minutes.

- 5 The x and y axis show the spatial coordinates in pixel values, where each pixel corresponds approximately to 1.2 arcsec. At  $t=0$  min the magnetic field around the PIL is very fragmented with very small positive and negative polarity regions randomly



distributed. These fragmented polarities start to coalesce forming at  $t=1920$  min a negative polarity region (N1), connected to the active region main negative polarity, and two smaller positive polarity regions, one northern of the negative polarity (P1) and other southern (P2). At  $t=2688$  min the positive polarities P1 and P2 coalesce with two smaller positive polarity regions that were located around them, indicated by red arrows in the figure. Later, at  $t=3072$  min, the positive polarity P2 connects to the active region main positive polarity. At  $t=4032$  min the negative polarity N1 starts to rotate clockwise around itself and the positive polarity P1 starts to rotate in the same sense around N1, moving between N1 and the active region leading negative polarity.

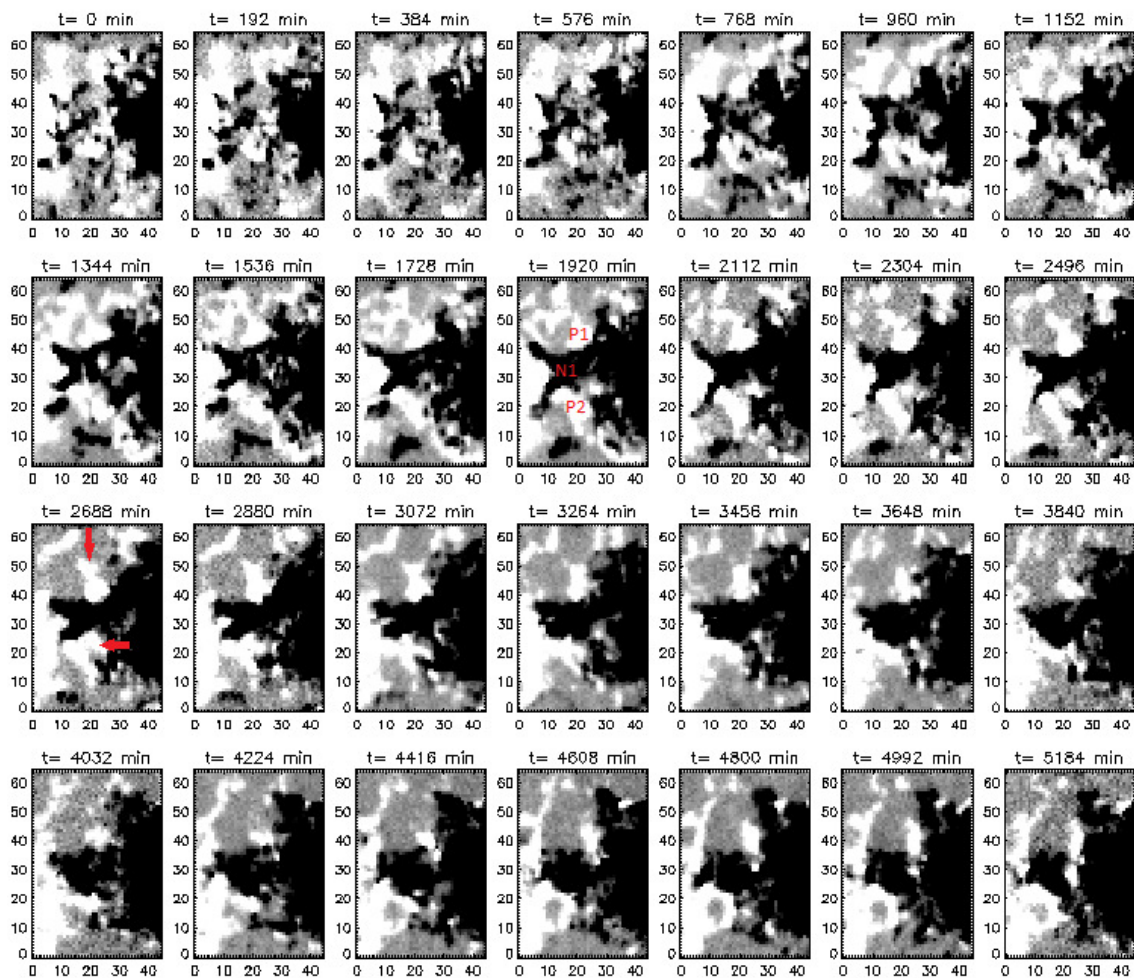


**Figure 2.** Evolution of the LOS component of the magnetic field around the PIL for the period of 3.6 days starting on December 31<sup>st</sup> 2000 at 01:34:43 UT.

To determine the velocity field responsible for the changes observed in the  $B_{LOS}$  component of the magnetic field, we have used the Local Correlation Tracking (LCT) technique (November and Simon, 1988). More specifically, we have used



a Fourier-based local correlation tracking (FLCT) implementation described in Welsch et al. (2004). We use the time of the sample of the  $B_{LOS}$  component ( $\approx 192$  min) and select a full width half maximum (FWHM) window of 5 pixel ( $\approx 6$  arcsec) to perform the localized cross-correlation. In applying the FLCT method we have considered  $B_{LOS}$  as a passive scalar and have assumed that all the changes observed in Figure 2 are due the horizontal displacement of the magnetic features, with no flux emergence or submergence.

## 2.1 Critical point detection and classification

In a 2D flow field the velocity vector is given at any point as  $\mathbf{v}(x, y) = v_x(x, y)\hat{i} + v_y(x, y)\hat{j}$ . If we consider a linear vector field approximation, the velocity vector components can be written in terms of the (x,y) coordinate components as

$$\begin{pmatrix} v_x(x, y) \\ v_y(x, y) \end{pmatrix} = \begin{pmatrix} a & b \\ \bar{a} & \bar{b} \end{pmatrix} \begin{pmatrix} x \\ y \end{pmatrix} + \begin{pmatrix} c \\ \bar{c} \end{pmatrix} \quad (1)$$

where

$$\mathbf{J} = \begin{pmatrix} a & b \\ \bar{a} & \bar{b} \end{pmatrix} \quad (2)$$

is the Jacobian matrix of the transformation.

So, to represent the velocity vector in a linear approximation we need to know the values of the constants  $a$ ,  $b$ ,  $c$ ,  $\bar{a}$ ,  $\bar{b}$  and  $\bar{c}$ . To find the values of the constants it is necessary to consider the velocity vector in at least three points around the region of interest (ROI), in order to solve the following linear system of equations

$$\begin{bmatrix} x_1 & y_1 & 1 \\ x_2 & y_2 & 1 \\ x_3 & y_3 & 1 \end{bmatrix} \times \begin{bmatrix} a \\ b \\ c \end{bmatrix} = \begin{bmatrix} v_x(x_1, y_1) \\ v_x(x_2, y_2) \\ v_x(x_3, y_3) \end{bmatrix} \quad (3)$$

for  $a$ ,  $b$ ,  $c$ , and the linear system of equations

$$\begin{bmatrix} x_1 & y_1 & 1 \\ x_2 & y_2 & 1 \\ x_3 & y_3 & 1 \end{bmatrix} \times \begin{bmatrix} \bar{a} \\ \bar{b} \\ \bar{c} \end{bmatrix} = \begin{bmatrix} v_y(x_1, y_1) \\ v_y(x_2, y_2) \\ v_y(x_3, y_3) \end{bmatrix} \quad (4)$$

for  $\bar{a}$ ,  $\bar{b}$  and  $\bar{c}$ . We solve the set of simultaneous linear equations of the form  $Ax = b$  by back-substitution using the IDL functions SVDC and SVSOL.

Once the linear representation of the field is available, we can use Equation 1 to check if there is a critical point inside the ROI. Critical points are the salient features of a flow pattern. Given a distribution of such a points and their types, much of the remaining geometry and topology of a flow field can be deduced. A critical point is characterized by a flow velocity given by



**Table 1.** Classification of critical points according to the values of the real (R) and imaginary (I) parts of the eigenvalues.

Critical point type	Real part of the eigenvalues	Imaginary part of the eigenvalues
Saddle point	$R1 < 0, R2 > 0$	$I1 = I2 = 0$
Attracting node	$R1, R2 < 0$	$I1 = I2 = 0$
Repelling node	$R1, R2 > 0$	$I1 = I2 = 0$
Attracting focus	$R1 = R2 < 0$	$I1 = -I2 <> 0$
Repelling focus	$R1 = R2 > 0$	$I1 = -I2 <> 0$
Center	$R1 = R2 = 0$	$I1 = -I2 <> 0$

$v(x, y) = (0, 0)_{ij}$ . Then, in a linear vector field approximation, to find the coordinates of the critical point we have to solve a matrix equation like

$$\begin{bmatrix} a & b \\ \bar{a} & \bar{b} \end{bmatrix} \times \begin{bmatrix} x \\ y \end{bmatrix} + \begin{bmatrix} c \\ \bar{c} \end{bmatrix} = \begin{bmatrix} 0 \\ 0 \end{bmatrix} \quad (5)$$

for  $x$  and  $y$ . The solution of this equation gives the  $(x, y)$  coordinates of the critical point, in case it exists.

5 From the eigenvalues of the Jacobian matrix, given by the solution of

$$\left| \begin{bmatrix} a & b \\ \bar{a} & \bar{b} \end{bmatrix} - \lambda \begin{bmatrix} 1 & 0 \\ 0 & 1 \end{bmatrix} \right| = 0, \quad (6)$$

we can classify the critical point, according to Helman and Hesselink (1989), as presented in Table 1. We find the eigenvalues by first reducing the Jacobian matrix to upper Hessenberg form using the ELMHES function in IDL and then returning the eigenvalues by applying the HQR function.

10 To automatically search for critical points, we scan the 2D LCT vector field using a rectangle of size  $(\Delta x, \Delta y)$ . The left panel on Figure 3 shows an illustration of the process for the vector field obtained at  $t=768$  min. Using the information of the flow and the coordinates at three corners of the rectangle, we perform the calculations described previously to search for critical points and classify them. By choosing different corners we cover the whole area inside the rectangle and after the calculation is finished we move the rectangle in the  $x$  direction by  $\Delta x$  and start the calculations again, until the end of the  
 15 line is reached. We then go to the next line by moving the rectangle  $\Delta y$  in the vertical direction until the complete 2D flow field is covered. The right panel on Figure 3 shows the result of this calculation where the asterisks indicate the position of the suggested critical points. The different colors indicate the classification of the critical points: blue–Saddle Point, red–Attracting Node/Focus and yellow–Repelling Node/Focus. The solid (dashed) contour line indicate the regions where  $B_{LOS}$  assumes the value of +100 G (-100 G). The results are sensitive to the size of the rectangle and should be cross checked by visual inspection  
 20 since the calculations may produce false positive cases or even miss some critical points. This cross check may be performed with the original 2D flow field, a re-normalized one or any visualization that could facilitate the identification of the critical points (LIC).

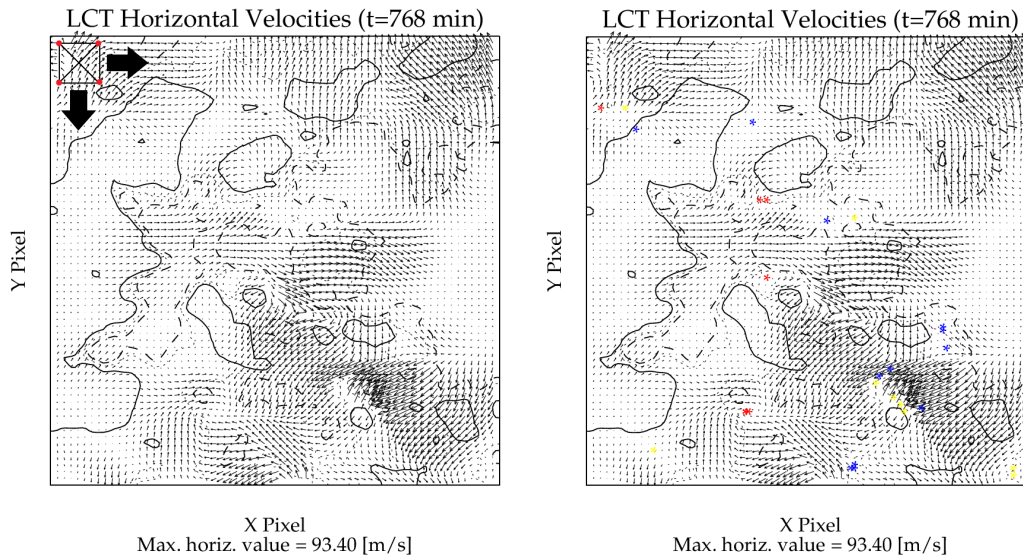


**Figure 3.** Left panel - Illustration of the method for automatic search of critical points in a 2D flow field. Right panel - results obtained using the automatic search for the LCT flow field at t=768 min. The asterisks show the location of the suggested critical points and the colors show their classification (blue: Saddle Point, red: Attracting Node/Focus, yellow: Repelling Node/Focus).

### 3 Results

Before we search for the presence of critical points in the flow field, we investigate the geometric aspect of the flow by calculating its fractal dimension. It describes how detail in a pattern changes with the scale at which is measured and provides a measure of geometrical complexity (Mandelbrot, 1982). To perform this calculation we apply a mask to the flow field, selecting only the regions where the velocity amplitude is larger than  $v = 23.6\text{m/s}$ . This value of velocity corresponds to the average of the velocities presented in the top panel of Figure 5. Figure 4 shows the time evolution of the distribution of the regions where the velocity amplitude is above the threshold, shown in black. We want to measure the fractal dimension of those structures.

The fractal dimension is calculated using the box counting method (Mandelbrot, 1982). The bottom panel of Figure 5 shows the results obtained for each time instant. They result in an average fractal dimension of  $\bar{D} = 1.63 \pm 0.05$ . This fractal dimension is very close to the one obtained for isotropic homogeneous turbulence ( $D = 5/3$ ), suggesting the occurrence of a turbulent flow around the PIL. Since fully developed turbulence consists of a hierarchy of eddies, we expect that vortex flows will be a common feature of the flow field around the PIL.

Next, we apply the method described in Section 2 to identify and classify the critical point candidates in the data cube containing the 2D LCT flow fields for the 3.6 days period, starting on December 31<sup>st</sup> 2000 at 01:34:43 UT. Before we apply the method, each flow field is re-sampled to have 128x128 data points. We select a rectangle of 2x2 to scan the flow field since

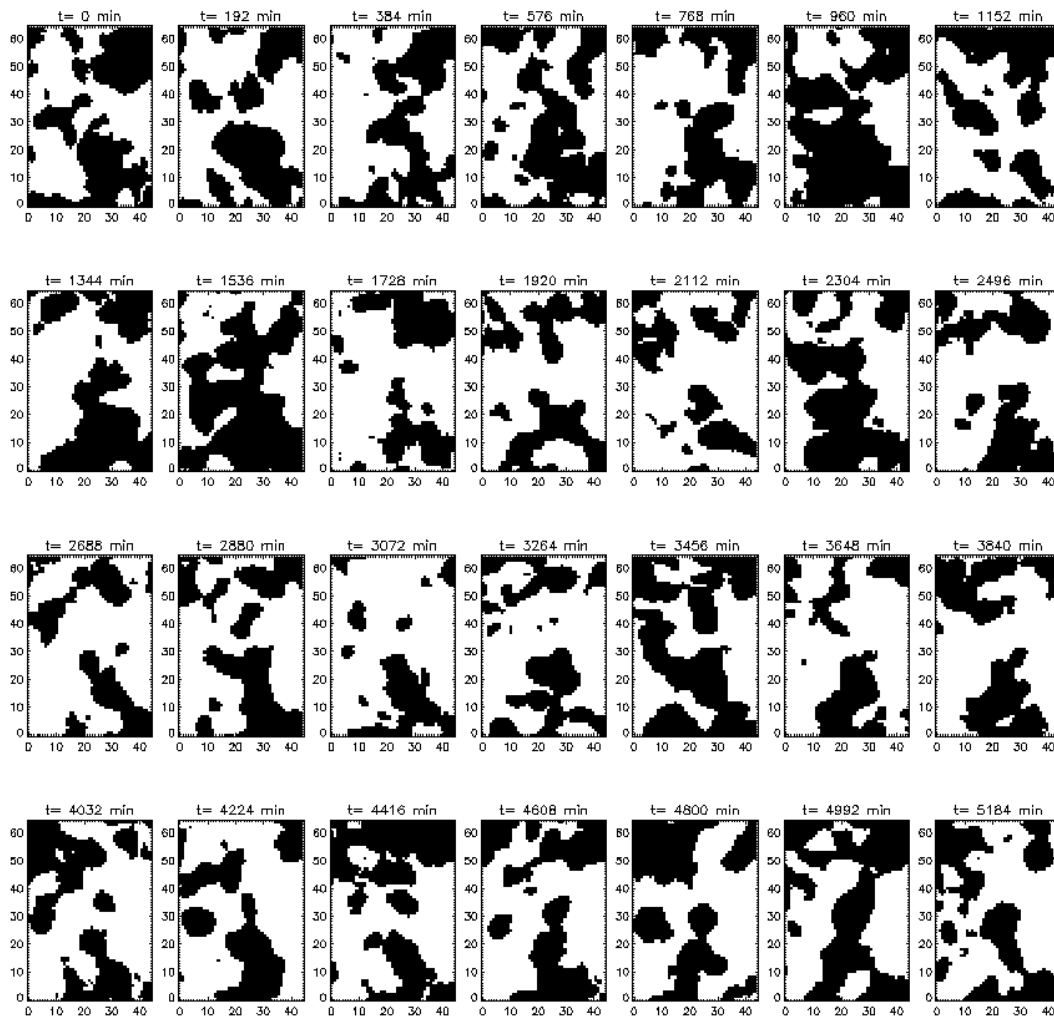


**Figure 4.** Time evolution of the regions where the velocity is above the threshold value of  $v = 23.6$  m/s, shown in black, for a period of 3.6 days starting on December 31<sup>st</sup> 2000 at 01:34:43 UT.

this is the resolution necessary to detect the smallest structures in the flow field. We select only the critical points classified as Attracting Focus and crosscheck the results with a flow field normalized in a way that all the flow vectors have the same sizes. These critical points are associated to vortex flows converging to them.

Figure 6 shows the 2D flow fields and the positions (red circle) where the presence of vortex flows were confirmed. We identified the occurrence of 12 (twelve) vortices in the LCT flow field obtained from the evolution of the LOS photospheric magnetic field around the PIL, for a period of 3.6 days. The arrows in Figure 6 show the direction of rotation, with about 67%

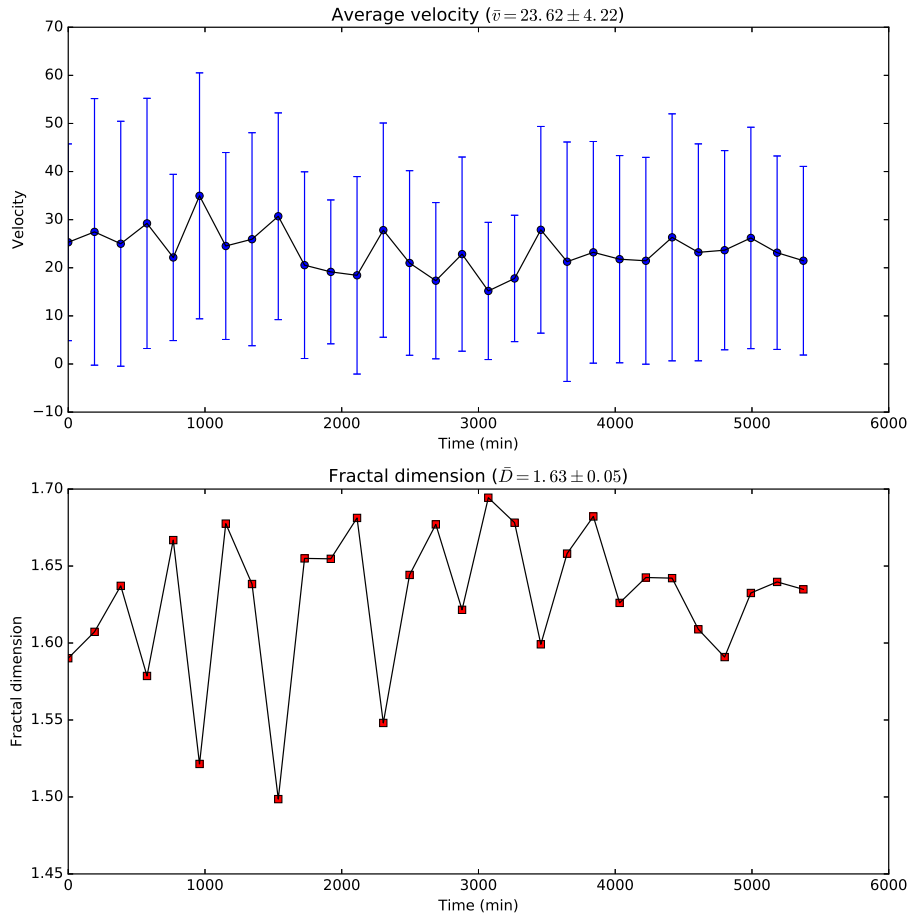


**Figure 5.** Temporal evolution of the average velocity (top panel) and fractal dimension (bottom panel) for the flow around the PIL.

(8) of the cases rotating clockwise and 33% (4) counterclockwise. This shows a preference to clockwise rotation in the set of vortices detected around the PIL.

Our investigation also shows that critical points are always present in the LCT flow fields for the period analyzed. Their total number varies with time and Saddle Points are the most commonly detected type of critical point. Figure 7 shows a rough estimation of the number of critical points obtained from our study. This results probably reflects the complexity of the flow field around the PIL since the lines connecting the critical points separate different flow regions.

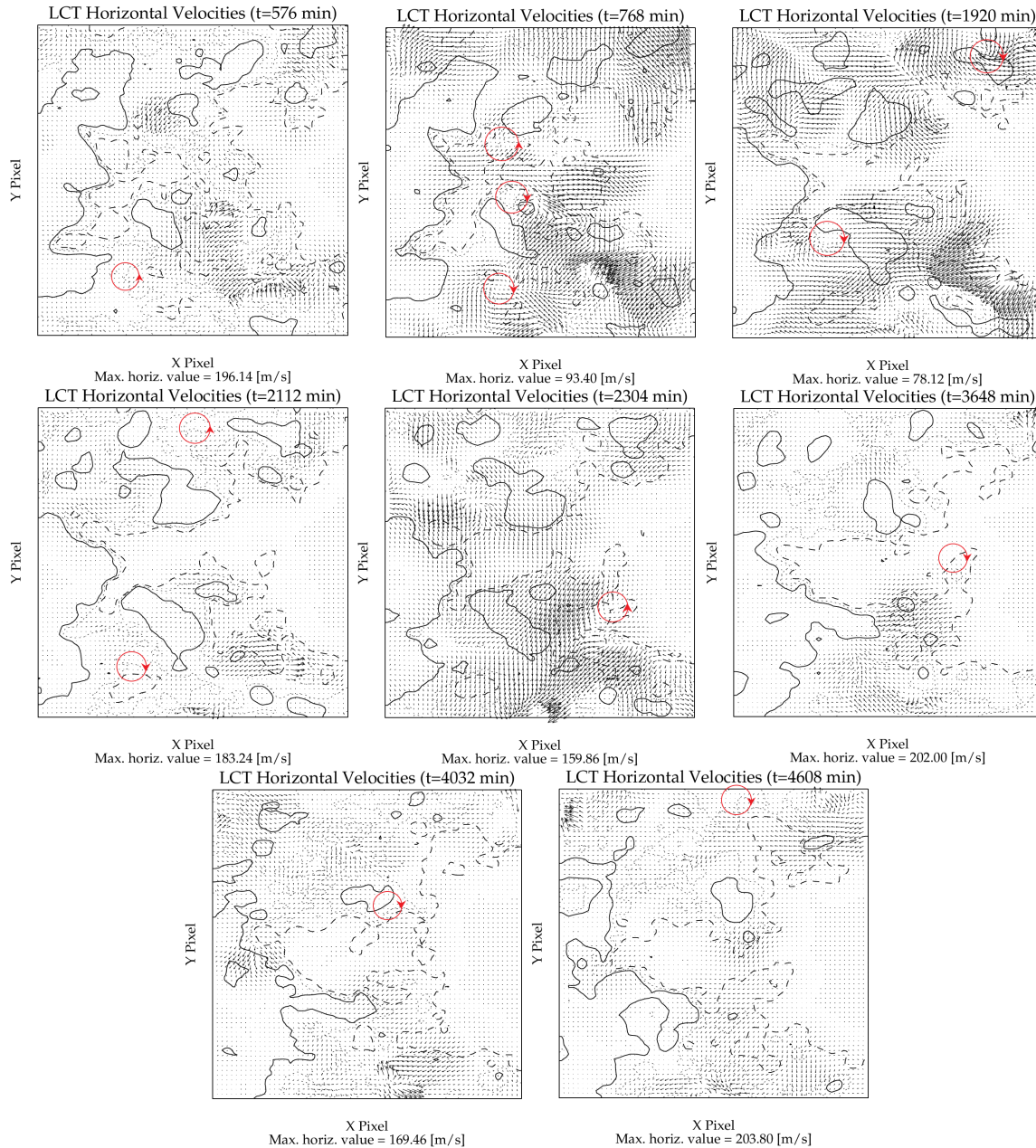


**Figure 6.** Location of the detected vortex flows in the 2D LCT flow fields obtained from the evolution of the magnetic structures around the PIL of a fully developed active region. The red circles indicate their location and the arrow indicate the direction of rotation.

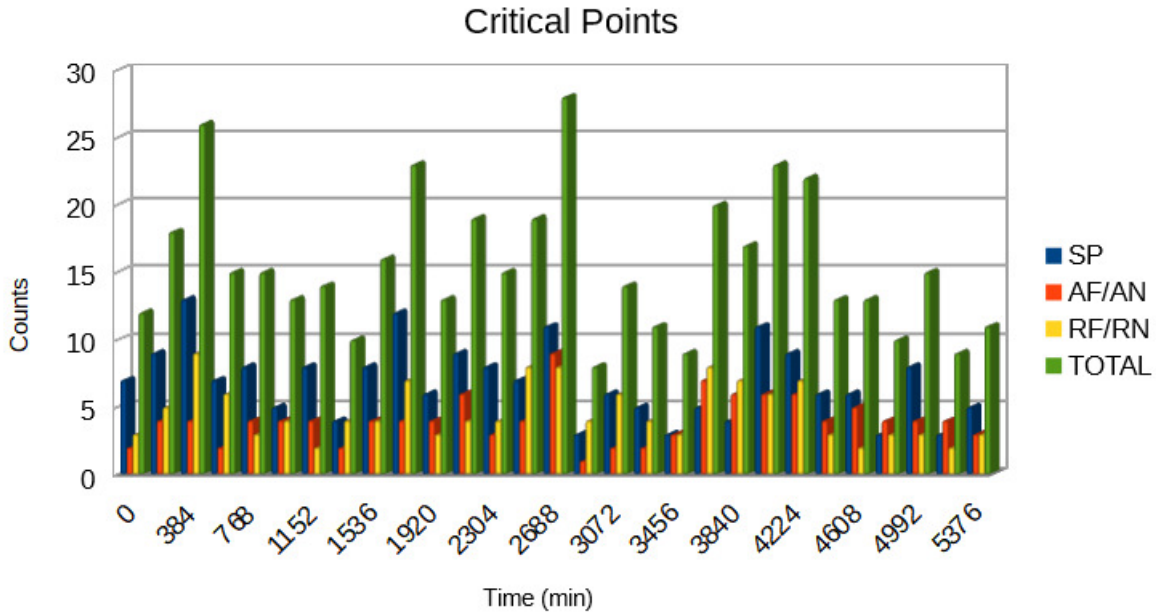


**Figure 7.** Counts of critical points detected on the 2D LCT flows obtained from the evolution of the magnetic field around the PIL for the period of 3.6 days.

#### 4 Conclusions

We have investigated the LCT flow fields obtained from the evolution of  $B_{LOS}$  in a region around the PIL for the presence of vortex flows. To perform this, we first look for the presence of critical points, using a linear approximation of the flow field, and classify them according to the eigenvalues of the Jacobian matrix of the linear transformation. Then, we sort a particular type of critical point called Attracting Focus which is associated to converging vortex flows. This procedure facilitates the visual identification of vortices in the 2D photospheric flow fields and in our results we have identified a total of twelve vortices in a period of 3.6 days. These vortices show a clockwise preferred sense of rotation with approximately 67% of the cases. Attracting Focus is not the only kind of critical point detected, with the most common type being Saddle Points. These results reveal the complexity of the flow field around the PIL and suggests, together with previous results, that vortex flows are indeed a relatively common feature in the solar photosphere. By calculating the fractal dimension of the regions where the velocity is larger than a threshold value of  $v = 23.6$  m/s, we obtain an average value of  $D = 1.62 \pm 0.05$ , which is very close to the values obtained for a homogeneous turbulence ( $D = 5/3$ ). This reinforces the complexity of the flow around the PIL, suggesting that it presents a turbulent nature.

Ann. Geophys. Discuss., <https://doi.org/10.5194/angeo-2019-33>

Manuscript under review for journal Ann. Geophys.

Discussion started: 19 March 2019

© Author(s) 2019. CC BY 4.0 License.



*Acknowledgements.* This work was supported by the CNPq under the project 307653/2017-0. J. C. Santos would like to thank the CNPq for the PCI-E2 postdoc fellowship under the individual project 300890/2017-6.



## References

- Attie, R., Innes, D. E., and Potts, H. E.: Evidence of photospheric vortex flows at supergranular junctions observed by FG/SOT (Hinode), , 493, L13–L16, <https://doi.org/10.1051/0004-6361:200811258>, 2009.
- 5 Balmaceda, L., Vargas Domínguez, S., Palacios, J., Cabello, I., and Domingo, V.: Evidence of small-scale magnetic concentrations dragged by vortex motion of solar photospheric plasma, , 513, L6, <https://doi.org/10.1051/0004-6361/200913584>, 2010.
- Bi, Y., Jiang, Y., Yang, J., Hong, J., Li, H., Yang, B., and Xu, Z.: Observation of a reversal of rotation in a sunspot during a solar flare, *Nature Communications*, 7, 13798, <https://doi.org/10.1038/ncomms13798>, 2016.
- Bonet, J. A., Márquez, I., Sánchez Almeida, J., Cabello, I., and Domingo, V.: Convectively Driven Vortex Flows in the Sun, , 687, L131, 10 <https://doi.org/10.1086/593329>, 2008.
- Bonet, J. A., Márquez, I., Sánchez Almeida, J., Palacios, J., Martínez Pillet, V., Solanki, S. K., del Toro Iniesta, J. C., Domingo, V., Berkefeld, T., Schmidt, W., Gandorfer, A., Barthol, P., and Knölker, M.: SUNRISE/IMaX Observations of Convectively Driven Vortex Flows in the Sun, , 723, L139–L143, <https://doi.org/10.1088/2041-8205/723/2/L139>, 2010.
- Brandt, P. N., Scharmer, G. B., Ferguson, S., Shine, R. A., and Tarbell, T. D.: Vortex flow in the solar photosphere, , 335, 238–240, 15 <https://doi.org/10.1038/335238a0>, 1988.
- Brown, D. S., Nightingale, R. W., Alexander, D., Schrijver, C. J., Metcalf, T. R., Shine, R. A., Title, A. M., and Wolfson, C. J.: Observations of Rotating Sunspots from TRACE, , 216, 79–108, <https://doi.org/10.1023/A:1026138413791>, 2003.
- Gopasyuk, O. S.: Rotation of sunspots in active region NOAA 10930, *Advances in Space Research*, 55, 937–941, <https://doi.org/10.1016/j.asr.2014.09.005>, 2015.
- 20 Hardersen, P. S., Balasubramaniam, K. S., and Shkolyar, S.: Chromospheric Mass Motions and Intrinsic Sunspot Rotations for NOAA Active Regions 10484, 10486, and 10488 Using ISOON Data, , 773, 60, <https://doi.org/10.1088/0004-637X/773/1/60>, 2013.
- Helman, J. and Hesselink, L.: Representation and display of vector field topology in fluid flow data sets, *Computer*, 22, 27–36, <https://doi.org/10.1109/2.35197>, 1989.
- Hiremath, K. M. and Suryanarayana, G. S.: The flares associated with the abnormal rotation rates of the bipolar sunspots: Reconnection probably below the surface, , 411, L497–L500, <https://doi.org/10.1051/0004-6361:20031618>, 2003.
- 25 Hiremath, K. M., Suryanarayana, G. S., and Lovely, M. R.: Flares associated with abnormal rotation rates: Longitudinal minimum separation of leading and following sunspots, , 437, 297–302, <https://doi.org/10.1051/0004-6361:20042495>, 2005.
- Jiang, Y., Zheng, R., Yang, J., Hong, J., Yi, B., and Yang, D.: Rapid Sunspot Rotation Associated with the X2.2 Flare on 2011 February 15, , 744, 50, <https://doi.org/10.1088/0004-637X/744/1/50>, 2012.
- 30 Kazachenko, M. D., Canfield, R. C., Longcope, D. W., and Qiu, J.: Sunspot Rotation, Flare Energetics, and Flux Rope Helicity: The Halloween Flare on 2003 October 28, , 722, 1539–1546, <https://doi.org/10.1088/0004-637X/722/2/1539>, 2010.
- Kosovichev, A. G. and Zharkova, V. V.: Magnetic Energy Release and Transients in the Solar Flare of 2000 July 14, , 550, L105–L108, <https://doi.org/10.1086/319484>, 2001.
- Li, A. and Liu, Y.: Sunspot Rotation and the M-Class Flare in Solar Active Region NOAA 11158, , 290, 2199–2209, 35 <https://doi.org/10.1007/s11207-015-0745-5>, 2015.
- Liu, C., Xu, Y., Cao, W., Deng, N., Lee, J., Hudson, H. S., Gary, D. E., Wang, J., Jing, J., and Wang, H.: Flare differentially rotates sunspot on Sun's surface, *Nature Communications*, 7, 13104, <https://doi.org/10.1038/ncomms13104>, 2016.
- Mandelbrot, B. B.: *The Fractal Geometry of Nature*, 1982.



- Min, S. and Chae, J.: The Rotating Sunspot in AR 10930, , 258, 203–217, <https://doi.org/10.1007/s11207-009-9425-7>, 2009.
- Moll, R., Cameron, R. H., and Schüssler, M.: Vortices, shocks, and heating in the solar photosphere: effect of a magnetic field, , 541, A68, <https://doi.org/10.1051/0004-6361/201218866>, 2012.
- 5 November, L. J. and Simon, G. W.: Precise proper-motion measurement of solar granulation, , 333, 427–442, <https://doi.org/10.1086/166758>, 1988.
- Ruan, G., Chen, Y., Wang, S., Zhang, H., Li, G., Jing, J., Su, J., Li, X., Xu, H., Du, G., and Wang, H.: A Solar Eruption Driven by Rapid Sunspot Rotation, , 784, 165, <https://doi.org/10.1088/0004-637X/784/2/165>, 2014.
- Scherrer, P. H., Bogart, R. S., Bush, R. I., Hoeksema, J. T., Kosovichev, A. G., Schou, J., Rosenberg, W., Springer, L., Tarbell, T. D., Title, A.,  
10 Wolfson, C. J., Zayer, I., and MDI Engineering Team: The Solar Oscillations Investigation - Michelson Doppler Imager, , 162, 129–188, <https://doi.org/10.1007/BF00733429>, 1995.
- Severnyi, A. B.: Nonstationary Processes in Solar Flares as a Manifestation of the Pinch Effect., , 2, 310, 1958.
- Sharykin, I. N., Sadykov, V. M., Kosovichev, A. G., Vargas-Dominguez, S., and Zimovets, I. V.: Flare Energy Release in the Lower Solar Atmosphere near the Magnetic Field Polarity Inversion Line, , 840, 84, <https://doi.org/10.3847/1538-4357/aa6dfd>, 2017.
- 15 Simon, G. W. and Weiss, N. O.: Kinematic Modeling of Vortices in the Solar Photosphere, , 489, 960–967, <https://doi.org/10.1086/304800>, 1997.
- Sudol, J. J. and Harvey, J. W.: Longitudinal Magnetic Field Changes Accompanying Solar Flares, , 635, 647–658, <https://doi.org/10.1086/497361>, 2005.
- Suryanarayana, G. S., Hiremath, K. M., Bagare, S. P., and Hegde, M.: Abnormal rotation rates of sunspots and durations of associated flares, , 580, A25, <https://doi.org/10.1051/0004-6361/201423389>, 2015.
- 20 Vargas Domínguez, S., Palacios, J., Balmaceda, L., Cabello, I., and Domingo, V.: Spatial distribution and statistical properties of small-scale convective vortex-like motions in a quiet-Sun region, , 416, 148–154, <https://doi.org/10.1111/j.1365-2966.2011.19048.x>, 2011.
- Vemareddy, P., Ambastha, A., and Maurya, R. A.: On the Role of Rotating Sunspots in the Activity of Solar Active Region NOAA 11158, , 761, 60, <https://doi.org/10.1088/0004-637X/761/1/60>, 2012.
- 25 Vemareddy, P., Cheng, X., and Ravindra, B.: Sunspot Rotation as a Driver of Major Solar Eruptions in the NOAA Active Region 12158, , 829, 24, <https://doi.org/10.3847/0004-637X/829/1/24>, 2016.
- Wang, H., Ewell, Jr., M. W., Zirin, H., and Ai, G.: Vector magnetic field changes associated with X-class flares, , 424, 436–443, <https://doi.org/10.1086/173901>, 1994.
- Wang, R., Liu, Y. D., Wiegmann, T., Cheng, X., Hu, H., and Yang, Z.: Relationship Between Sunspot Rotation and a Major Solar Eruption  
30 on 12 July 2012, , 291, 1159–1171, <https://doi.org/10.1007/s11207-016-0881-6>, 2016.
- Wang, S., Liu, C., Deng, N., and Wang, H.: Sudden Photospheric Motion and Sunspot Rotation Associated with the X2.2 Flare on 2011 February 15, , 782, L31, <https://doi.org/10.1088/2041-8205/782/2/L31>, 2014.
- Wedemeyer-Böhm, S. and Rouppe van der Voort, L.: Small-scale swirl events in the quiet Sun chromosphere, , 507, L9–L12, <https://doi.org/10.1051/0004-6361/200913380>, 2009.
- 35 Welsch, B. T., Fisher, G. H., Abnett, W. P., and Regnier, S.: ILCT: Recovering Photospheric Velocities from Magnetograms by Combining the Induction Equation with Local Correlation Tracking, , 610, 1148–1156, <https://doi.org/10.1086/421767>, 2004.
- Yan, X. L. and Qu, Z. Q.: Rapid rotation of a sunspot associated with flares, , 468, 1083–1088, <https://doi.org/10.1051/0004-6361:20077064>, 2007.



- Yan, X.-L., Qu, Z.-Q., and Kong, D.-F.: Relationship between rotating sunspots and flare productivity, , 391, 1887–1892, <https://doi.org/10.1111/j.1365-2966.2008.14002.x>, 2008.
- Yan, X.-L., Qu, Z.-Q., Xu, C.-L., Xue, Z.-K., and Kong, D.-F.: The causality between the rapid rotation of a sunspot and an X3.4 flare, *Research in Astronomy and Astrophysics*, 9, 596–602, <https://doi.org/10.1088/1674-4527/9/5/010>, 2009.
- 5 Yan, X. L., Qu, Z. Q., Kong, D. F., and Xu, C. L.: Sunspot Rotation, Sigmoidal Filament, Flare, and Coronal Mass Ejection: The Event on 2000 February 10, , 754, 16, <https://doi.org/10.1088/0004-637X/754/1/16>, 2012.
- Zhu, C., Alexander, D., and Tian, L.: Velocity Characteristics of Rotating Sunspots, , 278, 121–136, <https://doi.org/10.1007/s11207-011-9923-2>, 2012.
- 240